

Parallel generation and coding of a terahertz pulse train

Cite as: APL Photonics 7, 126105 (2022); <https://doi.org/10.1063/5.0123697>

Submitted: 31 August 2022 • Accepted: 22 November 2022 • Accepted Manuscript Online: 28 November 2022 • Published Online: 12 December 2022

 Joel Edouard Nkeck, Louis-Philip Béliveau,  Xavier Ropagnol, et al.

COLLECTIONS

 This paper was selected as an Editor's Pick



View Online



Export Citation



CrossMark

ARTICLES YOU MAY BE INTERESTED IN

[An ultra-fast liquid switch for terahertz radiation](#)

APL Photonics 7, 121302 (2022); <https://doi.org/10.1063/5.0130236>

[Thermally stable high numerical aperture integrated waveguides and couplers for the 3 \$\mu\text{m}\$ wavelength range](#)

APL Photonics 7, 126106 (2022); <https://doi.org/10.1063/5.0119961>

[Ultra-long Brillouin optical time-domain analyzer based on distortion compensating pulse and hybrid lumped-distributed amplification](#)

APL Photonics 7, 126107 (2022); <https://doi.org/10.1063/5.0126068>

Learn more and submit

APL Photonics

Applications now open for the
Early Career Editorial Advisory Board

Parallel generation and coding of a terahertz pulse train

Cite as: APL Photon. 7, 126105 (2022); doi: 10.1063/5.0123697
Submitted: 31 August 2022 • Accepted: 22 November 2022 •
Published Online: 12 December 2022



View Online



Export Citation



CrossMark

Joel Edouard Nkeck,¹  Louis-Philip Béliveau,¹ Xavier Ropagnol,^{1,2}  Dominic Deslandes,¹ 
Denis Morris,³  and François Blanchard^{1,a)} 

AFFILIATIONS

¹Département de Génie Électrique, École de Technologie Supérieure (ÉTS), Montréal, Québec H3C 1K3, Canada

²INRS – EMT Institut National de Recherche Scientifique, Varennes, Québec J3X 1P7, Canada

³Département de Physique, Université de Sherbrooke, Sherbrooke, Québec J1K 2X9, Canada

^{a)} Author to whom correspondence should be addressed: francois.blanchard@etsmtl.ca

ABSTRACT

The generation and coding of multi-cycle terahertz (THz) pulses offer interesting possibilities, such as frequency comb spectroscopy or ultrafast packet communication. In contrast to the radio frequency domain, which has largely exploited packet communication, this research area is almost unexplored at THz frequencies. Indeed, because of the lack of fast modulation and detection methods at THz frequencies, current developments often rely on hybrid techniques mixing photonics and ultrafast electronics. Here, we present a method for the generation and modulation of a coded THz pulse train. Our scheme is based on the combination of a spintronic THz emitter (STE) with an echelon mirror and a digital micromirror device. This highly scalable configuration is capable of modulating a hundred or more THz pulses in parallel with sub-picosecond accuracy. Strikingly, the temporal resolution of our modulation scheme depends on geometric optics and not on a high-speed electronic device. Furthermore, our scheme confirms the ability of STEs to generate quasi-continuous THz pulses and offers a new photonic solution on dynamic THz pulse train control.

© 2022 Author(s). All article content, except where otherwise noted, is licensed under a Creative Commons Attribution (CC BY) license (<http://creativecommons.org/licenses/by/4.0/>). <https://doi.org/10.1063/5.0123697>

I. INTRODUCTION

Officially, since 2019, the terahertz (THz) band (>100 GHz) has been considered the next frontier of wireless communications for Beyond-5G (B5G) and 6G networks, more specifically, for the frequency range between 95 GHz and 3 THz.¹ Although this official status was only granted recently, researchers have been actively exploring this range of electromagnetic frequencies for decades^{2,3} and, in the process, have realized considerable progress in generating^{4–7} and detecting^{8–11} these waves to satisfy various application areas, including ultrafast spectroscopy,^{5,12,13} biomedicine,^{14,15} and security.^{16,17} With the recent increased attention to THz communications, several approaches based on electronic and photonic solutions are currently the subject of intensive research and development.^{18–20} One of the current key elements of a photonic solution is the THz photomixer,²¹ which generates continuous waves with modulation capability in the GHz range through a radio frequency modulator.²² To bypass high-speed electronics, the shaping of THz pulses

generated by a femtosecond (fs) laser has long been considered,^{23,24} especially keeping in mind that fs lasers will become more and more accessible and miniature in the coming years.²⁵ This aspect will undoubtedly allow the development of unique solutions based on quantum photonics sensing²⁶ and could open new possibilities for THz communications.

Optical pulse shaping²⁴ of a pump beam has enabled the generation and modulation of ultrafast THz pulses through various approaches, such as metamaterial-based devices,^{27–30} with the use of photoconductive antennas^{23,31} or nonlinear crystals,^{32–34} liquid crystals,³⁵ photo-injected charge carriers in waveguides for phase-controlled pulse trains,³⁶ and via the Vernier effect in a regenerative amplifier.³⁷ Recent work has also demonstrated the encoding of THz pulses by a passive diffractive device where the amplitude and phase of the input wavelengths are independently controlled.³⁸ Unfortunately, most of these approaches^{23,27–35,37,38} are able to generate THz pulses with sub-picosecond accuracy but without dynamic modulation capability, while other approaches are largely limited in the

number of output pulses generated and have the additional challenge of free-space coupling.³⁶ To date, a simple dynamic pulse train generator with sub-picosecond time resolution parallel modulation remains an unsolved challenge but undeniably represents an important playground for promising new advances.

Here, we report on the generation and manipulation of a THz pulse train using a combination of an echelon mirror, a digital micromirror device (DMD), and a spintronic broadband THz emitter (STE).³⁹ The echelon mirror sets the carrier frequency of the envelope of the pulse train, and the DMD behaves as an active space-time light modulator. Our results show the efficient generation of a THz pulse train consisting of up to 128 pulses, dictated by the number of mirror steps irradiated by the pump beam on the step mirror. After the reflection on this step mirror, the successive projection of the optical pumping beam on the DMD surface and its focus on a spintronic type emitter allows the generation and the modulation in parallel of the THz pulse train. The spatiotemporal relationship between the pulses actively selected by the DMD converted into THz pulses in the STE provides sub-picosecond modulation accuracy, which depends mainly on the quality of the step mirror image projected onto the DMD. With the on-off-keying (OOK) pulse modulation scheme, we show two 24- and 64-bit coded digital words using three- and one-pulse protocols, respectively. This novel demonstration may open the door to future packet communication protocols using THz waves without the requirement of an ultrafast electronic device.

II. MATERIALS AND METHODS

A. THz time domain setup

Figure 1(a) shows a schematic of the experimental setup. The laser used in this experiment was the oscillator femtosecond

Chameleon Discovery NX laser from Coherent, Inc. company, delivering sub-100 fs optical pulses with tunable wavelengths ranging from 660 nm to 1320 nm, at a repetition rate of 80 MHz, with an average output power around 3 W at 800 nm. For the requirements of the experiment, we set the laser wavelength to 800 nm. For this pump-probe experiment setup, the laser beam was split into two using a 90:10 beam splitter with 90% of the optical power sent into the pump beam for the generation of the pulse train and the THz radiation, while 10% was sent into the probe beam for THz detection via photoconductive sampling. The THz detector was a low temperature GaAs photoconductive antenna from Teravil, with a hyperhemispherical high resistivity silicon lens on the back of the antenna. This detector is optimized for a collimated THz beam with a diameter smaller than 12 mm.

As described in Sec. III, the pulse train is comprised of an echelon mirror, an optical polarization switch, and a beam expander (BE). As it is essential that the optical beam is normal to the surface of the echelon, the round trip through a quarter-wave plate converts the horizontally polarized input light into vertically polarized output light (i.e., after reflection on the echelon mirror), which, in turn, converts a reflection into a transmission on the PBS cube, the so-called optical switch. In order to illuminate the whole area of the echelon, the BE increases the optical beam size and then maximizes the number of generated optical pulses in the pulse train. The echelon mirror is a Ni-P stepped mirror from Sodick F.T. Co., with a 150 μm wide and 75 μm high step, generating a time delay between two consecutive beamlets of 1 ps and 500 fs, depending on the illuminated side. Then, the optical pulse train is imaged onto a digital microdevice mirror (DMD) DLP4500.45 WXGA from Ajile, which is an active modulator, to pattern the input wave packet. To be able to carry out the modulation shaping of the pulse train, we ensure to image the echelon mirror onto the DMD by using a $\times 2$ microscope objective lens. The pulse train is then guided and focused onto the STE

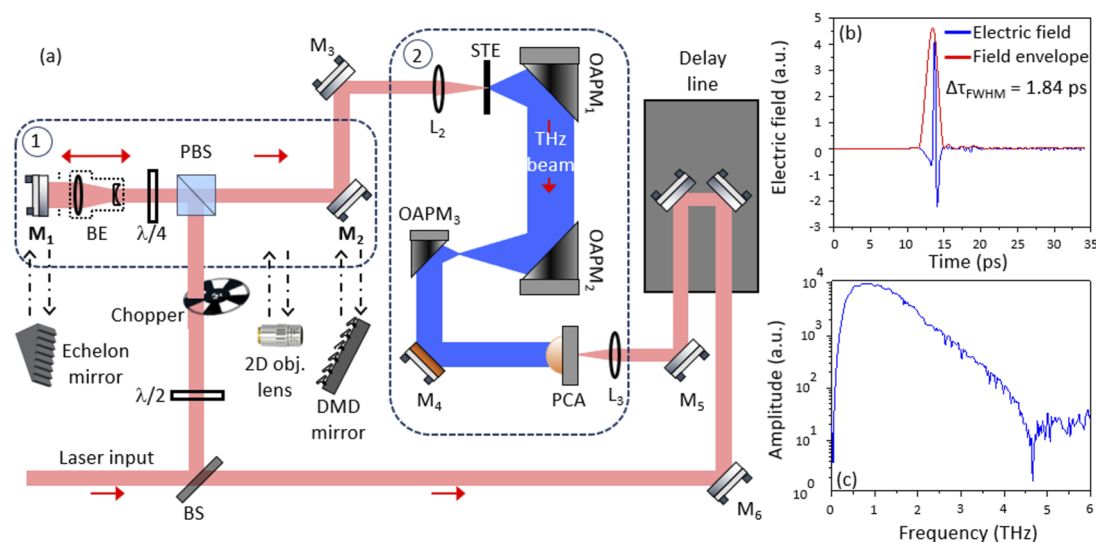


FIG. 1. Experimental setup. (a) Experimental setup for THz generation using STE: (1) system where mirrors M_1 and M_2 can be replaced by the echelon mirror and DMD mirror, respectively, and (2) generation and detection system in a purged box. (b) Time domain and field envelope of the generated transient THz pulse. (c) Fourier transform of the THz pulse.

trilayer ($W/Co_{0.5}Fe_{0.35}B_{0.15}/Pt$), which is placed between two magnets whose applied magnetic field is parallel to the plane of the laboratory frame. This magnetic field, which is perpendicular to the direction of the pulse train, determines the polarization of the THz electric field, which is perpendicular to it.³⁹

The THz beam is collected and guided by off-axis parabolic mirrors (OAPM). First, it is collimated with a 2-in. diameter and focal length OAPM₁. Then, the THz beam is sent to a telescope made of 2 OAPM for collimating the THz beam and reducing the beam size down to a 12 mm diameter. The 2 OAPM forming the telescope are, respectively, 2 in. and 1 in. in diameter and 3 in. and 1 in. in focal length. After the telescope section, a flat gold mirror guides the collimated THz beam onto the antenna detector. It should be noted that the pump beam is mechanically chopped at a 2 kHz frequency to allow a lock-in detection when the modulation of the DMD is not used. In addition, we purged the THz beam path with dry air to avoid absorption by water vapor.

B. Spintronic terahertz emitter (STE): Fabrication

The spintronic emitter consists of a stack of three layers ($W/Co_{0.5}Fe_{0.35}B_{0.15}/Pt$) composed of two heterostructures between a non-ferromagnetic metal and a ferromagnetic metal. The thickness of each metallic film is about 2 nm. All the layers were obtained in the same thin film deposition chamber (IntelVac, Nanochrome I) with a bare pressure of 3×10^{-7} mbar on 25 mm diameter and 350 μm thickness quartz substrates. The organic contaminants of the substrate were first removed via a standard solvent cleaning procedure (acetone 5 min and isopropyl alcohol 5 min) that was followed by an ex-situ plasma etching using oxygen (100 W, 5 min.) and an *in situ* Ar-plasma etch (10 sccm, 10 min). The tungsten (W) layer was deposited by sputtering at a rate of about 2.2 $\text{\AA}/\text{s}$, at a deposition pressure of 3×10^{-3} mbar. The cobalt-iron-boron alloy ($Co_{0.5}Fe_{0.35}B_{0.15}$) and the platinum (Pt) layers were deposited by e-beam evaporation at a rate of about 0.5 $\text{\AA}/\text{s}$. The emitter was mounted on a non-magnetic holder between two magnet poles, which allowed applying fields up to 100 mT in the plane of the sample along the X-axis of the laboratory frame.

The principle of THz generation is based on the transfer of a spin current to an ultrafast charge current by the inverse spin Hall effect (ISHE).³⁹ Hence, the optical pump beam excites spin-polarized electrons in the magnetic layer ($Co_{0.5}Fe_{0.35}B_{0.15}$), giving rise to a spin current, which, in turn, excites a transverse transient

electric current in the W and Pt layers. The variation of this transient current generates a THz pulse emitted in the forward and backward directions of the spintronic's plan.

III. RESULTS

A. Experimental configuration and THz pulse train generation

The lower part of Fig. 2(a) illustrates the process of generation of the train of optical pulses by the illumination of an echelon mirror measuring $20 \times 10 \text{ mm}^2$ in size and having 150 μm wide and 75 μm high pitches. To achieve an illumination with 0 degrees of incidence on the echelon mirror, an optical switch, composed of a polarizer beam splitter cube and a quarter-wave plate, is used (see Sec. II). Before reaching the step mirror, a $\times 2$ to $\times 8$ variable beam expander (BE) (Edmund Optics model 87-570) is inserted into the pump beam path. This configuration has the double advantage of allowing an adjustment of the number of steps illuminated while maintaining constant the size of the pump beam at the exit of the polarizer cube. To validate the magnification and the position of the echelon, we imaged the steps of the echelon mirror using the $\times 2$ apochromatic microscope objective lens (model 46-142 from Edmund Optics) on a charge coupled device (CCD) camera model DCC3240M from Thorlabs. The top part of Fig. 2(a) shows the 3D top view of the echelon mirror and the image obtained from the echelon mirror. In the zoomed-in view, we can see that three steps correspond approximately to 230 μm on the CCD image, the equivalent of a magnification of 1 at the image plane.

In the bottom illustration of Fig. 2(b), the DMD is inserted at the image plane of the $\times 2$ lens. To ensure that the DMD is correctly positioned in the image plane, a second apochromatic $\times 5$ lens (Mitutoyo MY5X-822) is used to relay the image reflected from the DMD to the CCD camera. To validate the exact position of the DMD with respect to the image plane of the $\times 2$ lens, a horizontal pattern of lines and spaces (i.e., in the x direction) is applied to the DMD (see supplementary material S1 for more details). As can be seen in the upper part of Fig. 1(b), the echelon image, together with the mask formation on the DMD, is well overlapped, i.e., the echelon image plane matches the DMD image position. In the zoomed-in view, we determined through measurement that the image of three steps from the echelon is projected onto an area corresponding to 21 active micromirrors.

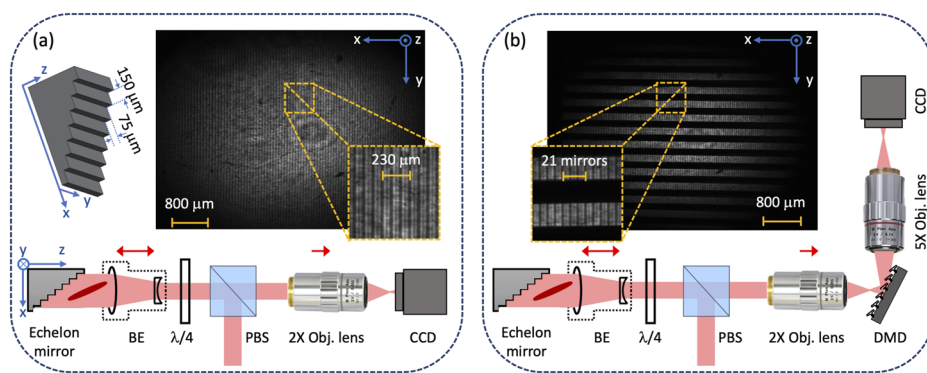


FIG. 2. Calibration and imaging of the steps of echelon on the digital microdevice (DMD) using a CCD camera. (a) Obtention of the image of the echelon mirror steps. (b) Image of the echelon mirror steps on the DMD. BE is a beam expander, $\lambda/4$ is a quarter-wave plate, PBS is a polarizer beam splitter cube, CCD is a charged couple device camera, and DMD is a digital micromirror device.

To date, echelon mirrors have mainly been used for single-shot time-domain THz spectroscopy^{40,41} and for the development of intense THz sources using the tilted-pulse front-pumping (TPFP) scheme.^{7,42} The idea behind using an echelon mirror is to temporally shape the reflected optical pulse at different delay times without dispersion, i.e., while preserving the ultrashort property for each reflected optical beamlet. For single-shot THz spectroscopy, the idea is to instantaneously probe each part of a THz pulse with a segmented ultrashort probing beamlet.^{40,41} In the case of intense THz generation using the TFPF configuration, a tilted pulse must be generated at the image plane in order to meet the phase matching condition inside a lithium niobate crystal along the Cherenkov angle.^{7,42} Interestingly, the DMD can also act as an active echelon mirror for ultrafast pulse measurements⁴³ and the TFPF scheme.⁴⁴ However, in contrast to previous studies,^{7,40–44} we are interested in converting each ultrafast optical beam into a single THz pulse train at a specific carrier frequency, thus generating a fixed frequency pulse train.

To perform the task of converting a two-dimensional spread beamlet to a consecutive series of optical pulses, a single optical lens is used. Temporally delayed by the height of each step of the echelon mirror, the beamlets, after passing through the lens, undergo a different temporal delay at the focal point. To validate this time combining assumption at the focal point, we performed finite difference time domain (FDTD) simulations using the Lumerical software. Figures 3(a)–3(e) show time snapshots of a femtosecond laser beam after reflection from a stair-step metal surface. This reflected beam

is transferred to a biconvex lens, and a monitor placed at the focus of this lens reveals the temporal passage of these beamlets (see the full-length simulation in video S2 of the [supplementary material](#)). In Figs. 3(a) and 3(b), we can see that pumping the step mirror on the 75 μm high side changes the initial 100 fs optical pump pulses to an optical wave packet with a temporal separation of 500 fs. Being non-dispersive, each wave packet, after reflection on the echelon mirror, preserves a duration of 100 fs for the entire simulation propagation. As can be seen in the last time map (e) of this figure, the short femtosecond laser pulses are separated in time and pass through the same location at the focus.

For THz wave generation via optical rectification in bulk nonlinear crystals, the phase matching condition between the pump light and the generated THz beam is essential to achieve good conversion efficiency.^{7,42} With our method, the image aberration and the tilt of the step mirror projection may cause an additional problem in obtaining a good phase matching condition if a thick bulk nonlinear crystal emitter is used. In order to overcome this possible restrictive condition, here, we used the recently developed spintronic THz emitter (STE).³⁹ Because it is made of thin films, this device is practically insensitive to phase matching conditions and alignment. In addition, the generation of long pulse trains can also represent a significant problem when the generating mechanism produces an echo from its finite thickness. Again, the STE can be positioned such as to prevent the presence of this echo from being a nuisance and is, therefore, a prime candidate for our application. Note that the generation of a second THz pulse, caused by a reflection on the air–substrate

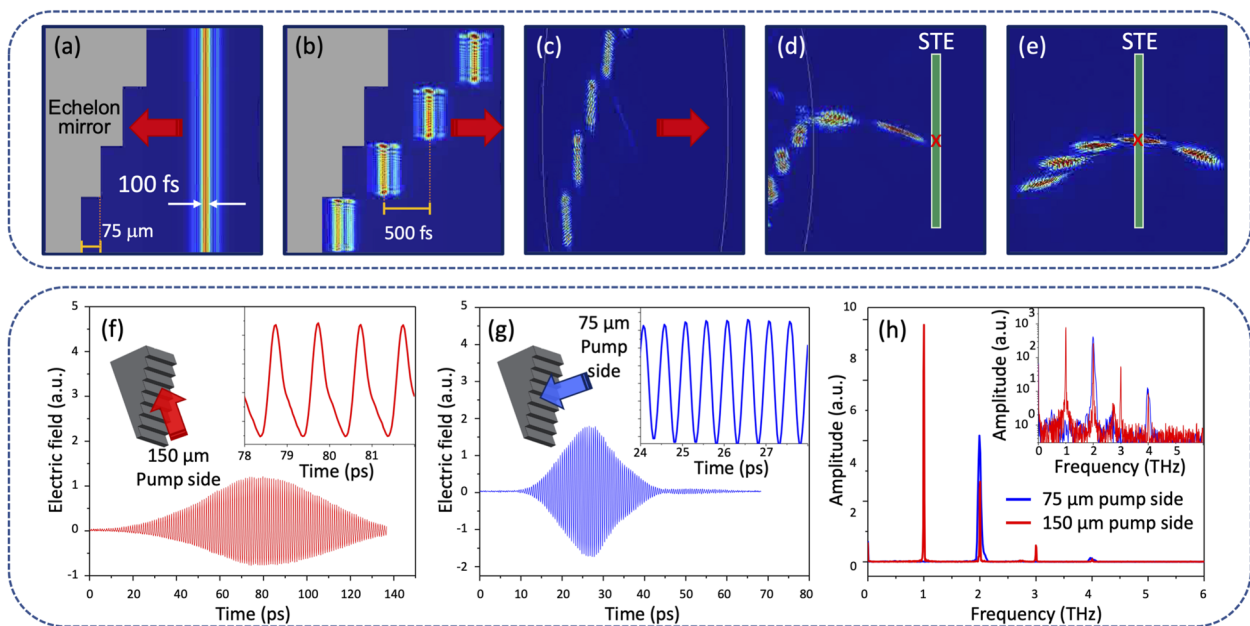


FIG. 3. Generation of pulse train using an echelon mirror. (a–e) Simulation, using FDTD software, of the 100 fs optical pulse through the system based on the echelon mirror, biconvex lens, and spintronic emitter (STE). The red arrow represents the direction of the optical pulse, and the red cross is the focal point. (f) Terahertz pulse train obtained by pumping on 150 μm side steps. The inset is the zoom on the THz time domain pulse train. (g) Terahertz pulse train obtained by pumping on 75 μm side steps. The inset is the zoom on the THz time domain pulse train. (h) Fourier transform of the THz time domain pulse train using 150 μm pump side (red) and 75 μm pump side (blue). In the inset, the frequency comb generated at 1 THz (red) and at 2 THz (blue) in the y-logarithm scale using 150 μm pump side and 75 μm pump side, respectively.

interface, is minimized when the structure is pumped from the metal side.⁴⁵

In Figs. 3(f) and 3(g), we show the results of generating two THz pulse trains obtained when the step mirror is illuminated on the facet with step heights of 150 μm and 75 μm , respectively. The respective insets to these figures represent a zoomed-in view of these pulse trains. In the inset, the time domain traces of the THz pulse train obtained with the 75 μm steps look like a quasi-perfect sine wave. However, looking at the whole set of time domain traces, we can clearly see an envelope with a Gaussian profile, which corresponds to the intensity profile of the pumping beam. In addition, in Fig. 3(f), approximately 128 pulses were generated over a maximum of 133 pulses according to the illuminated size of our echelon mirror and its step size corresponding to 4.85 mm beam size at full width at half maximum (FWHM). In Fig. 3(g), approximately 72 pulses has been generated, which correspond to a beam size of 2.7 mm at FWHM.

In Fig. 3(h), the frequency spectra of both pulse trains show a strong peak located at 1 THz (red) and 2 THz (blue), with a bandwidth at a FWHM of 13 GHz and 60 GHz, respectively. Since the STE produces broadband THz pulses, the Fourier transform of these pulse trains also produces the harmonics corresponding to the initial carrier frequency of the two pumping conditions, i.e., pumping on the facets with step heights of 150 and 75 μm , respectively. In both cases of excitation of the echelon mirror, we perceive a small replica of up to 4 THz, limited by the bandwidth of our THz detector as explained in Sec. II. The inset in Fig. 3(h) shows the same frequency spectrum on a logarithmic scale. It is striking to note the very narrow bandwidth of our pulse train generation mechanism. Specifically, we estimate the Q-factor of these frequency combs to be 86 and 51 for pulse trains centered at 1 and 2 THz, respectively, which is about 10 times sharper than the recently reported THz pulse trains.³⁶

B. Parallel modulation and coding

As mentioned earlier, varying the diameter of the pump beam using the beam expander changes the number of steps illuminated on the echelon mirror, which results in changes of the number of THz cycles generated in the time domain but with no changes of the carrier frequency of the emitted pulse train. Therefore, we can fine tune the duration of the THz pulse train by simply changing the illumination size on the echelon (i.e., by changing the number of illuminated steps). For the following experiments, we reduced the diameter of the pumped optical beam to 3.17 mm at FWHM and illuminated the 150 μm side, corresponding to a carrier frequency of 1 THz. In Fig. S3(a), we show the intensity profile extract from Fig. S1(a) of the step image, and Fig. S3(b) shows its corresponding generated THz pulse train. These results clearly show that each generated THz pulse corresponds to a step position of the echelon, which is in agreement with the simulations in Fig. 3. We noticed that due to the angle of incidence of the pump on the echelon mirror and the sharpness performance of the apochromatic lens, which had a depth of field of a few micrometers, the edges of the image appeared blurred, while the center was perfectly imaged. As we will see in the next paragraph, a blurred image on the DMD loses precision on the pulse modulation.

By using the DMD with vertical line patterns instead of the horizontal lines used in the alignment procedure in Fig. 2(b), each step of the echelon mirror can be imaged on the DMD and selected (or not selected) on demand by simply activating the micromirrors. In Fig. 4, we show an example of pulse separation using some vertical line and space patterns (i.e., in the y direction) applied on the DMD. Figures 4(a)–4(c) show the line and space patterns for a selected series of 13, 10, and 5 on and off pulses, respectively. The zoomed-in top view clearly shows the precision of the pulse selection as well as the high signal-to-noise ratio (SNR) of this demonstration in the central part of the pulse train. Indeed, the peripheral positions of the pulse train have a lower SNR than its central part, but this problem could be circumvented by using an appropriate shaping of the pump beam in square shape and top hat intensity.⁴⁶

To demonstrate the range of control of the THz pulse train, the DMD also allows each THz pulse to be individually coded via a seven micromirror wide vertical line. For this demonstration, we used the ASCII binary protocol and on–off keying modulation. In the ASCII code, each character is produced from 8 bits. In fact, the pump light reflected from each individual step of the echelon mirror can be actively turned on or off at the DMD image plane, as long as the echelon image remains defined to a precision on the order of a DMD mirror size (i.e., accuracy on the order of about ten micrometers or better). To simplify the understanding of our first test, we used 3 THz pulses per bit to generate the three letters forming the word “ETS.” Figure 5(a) shows the result obtained for the 72 modulated pulses in an OOK 3 pulses per bit protocol. The corresponding binary pattern is <0100 0101 0101 0100 0101 0011>. The signal is clearly observable and understandable from a binary point of view with a Gaussian-shaped amplitude vs time profile. In Fig. 5(b), we go to the limit of the OOK protocol by modulating each THz pulse for one bit. With 64 pulses for this demonstration, we encoded the eight letters: “ETS2021!,” corresponding to the bit pattern: <0100 0101 0101 0100 0101 0011 0011 0010 0011 0000 0011 0010 0011 0001 0010 0001>. Indeed, this experiment was first done in 2021. For both of these OOK modulation results, the carrier frequency remains stable at 1 THz, but we note that the pulse-coded THz signal using the three-pulse scheme [Fig. 5(a)] is more readable compared to the single-pulse coded signal [Fig. 5(b)], confirming the importance of the pump beam image quality at the DMD position. As can be noted, the central part of Fig. 5(b) shows a clear contrast between the transported on and off information of the THz pulses, while the peripheral positions become more blurred and more difficult to discretize. As mentioned above, the reason why the information is less legible at the edges of the beam (or for the beginning and end of the pulse train) is directly related to the imaging conditions and not to the speed of an electronic component (see [supplementary material S3](#) for more details). This is important to note because this ultrafast modulation is not related to a fast electronic process but, rather, is only dictated by geometric optics. One way to circumvent this problem would be to use a suitable mask on the DMD. Since the edge of the step image on the DMD is blurred, a larger modulation area should be used, e.g., having lines and spaces matched according to the position on the DMD. Another approach would be to design an imaging solution capable of imaging an inclined plane with a larger working distance, especially for the imaged plane of the echelon.

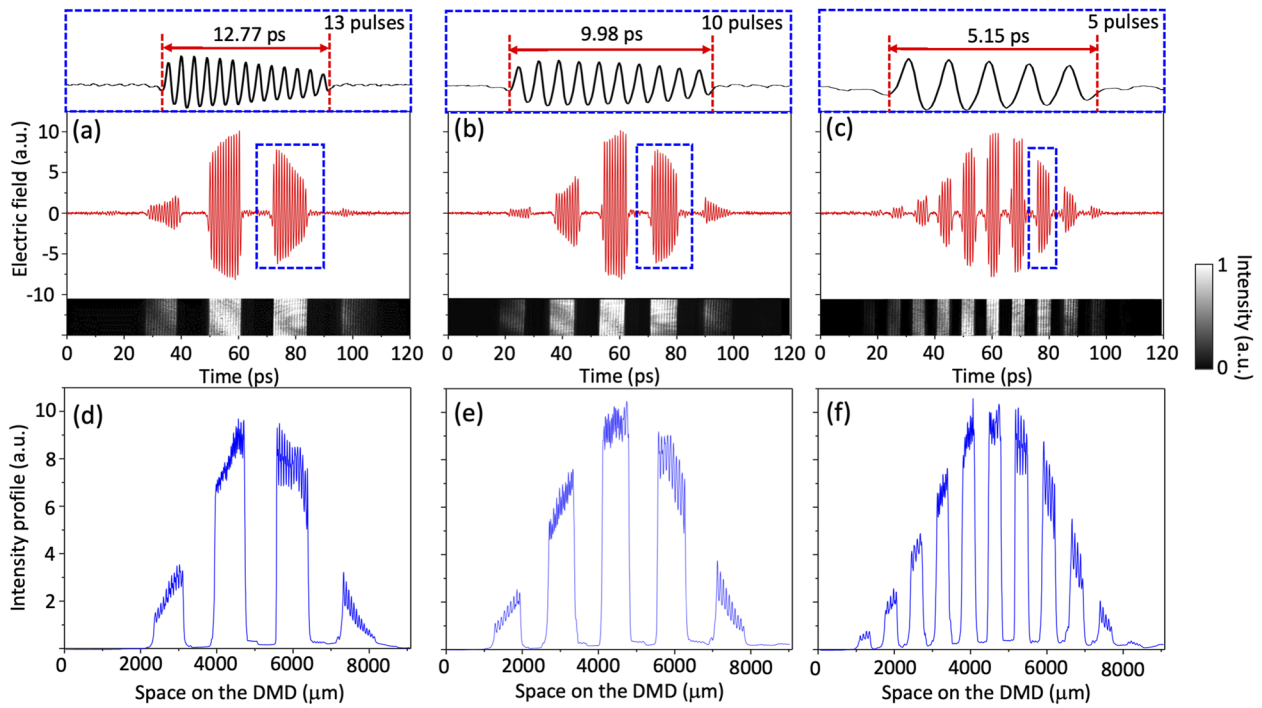


FIG. 4. Control of the number of pulses with respect to the image configuration pattern on the DMD. Packet generation of (a) 13 pulses, (b) 10 pulses, and (c) 5 pulses and their intensity images after the passage on the DMD presented on the lower part of the figure. Intensity profile of images corresponding to (d) 13 pulses, (e) 10 pulses, and (f) 5 pulses.

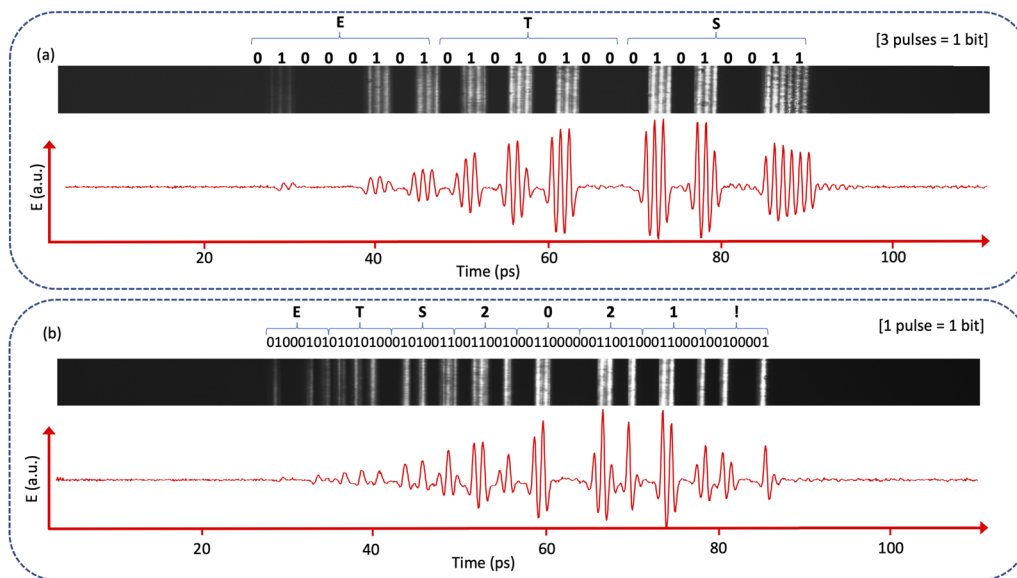


FIG. 5. (a) THz pulse train encoding of (a) ETS by considering three pulses as 1 bit and (b) ETS2021! by considering one pulse as 1 bit with respect to the imaging configuration pattern on DMD.

IV. DISCUSSION

We have demonstrated the generation and the modulation of a THz pulse train using the combination of an echelon mirror, a DMD, and an STE. Our proposed modulation scheme accurately converts the spatial information of the pump beam into the temporal information of a pulse train at the carrier frequency of 1 THz. Strikingly, the sub-picosecond modulation accuracy is only limited by geometric optics, thus eliminating the need for an ultrafast electronic component.

The actual limitation of our method lies in the use of a DMD, which does not allow to modulate the pump beam faster than 6 kHz. Considering the number of pulses generated (i.e., 128 pulses) and a modulation rate for an OOK encoding, our system currently allows us to transport 768 kb/s. This data transfer rate can be increased by replacing the DMD by an electro-optic modulator existing in the literature⁴⁷ and capable of tracking each pulse of the laser at a rate of 80 MHz.

Finally, it should be noted that our demonstration was performed using a time-domain spectroscopy system coupled to a delay line, which at this time is clearly not intended for ultrafast real-time signal acquisition and, thus, incompatible with a THz communication application. Nevertheless, there would be possible solutions to increase the data transfer rate, which is not the purpose of our article. Since the first demonstrations of THz communications,⁴⁸ photonics has played a key role in the development of emitters and detectors. On the other hand, electronics-based approaches are still more efficient for realizing sources and receivers whose applications will mainly involve continuous THz waves.¹⁸ Today, we are still far from democratizing THz communications due to the enormous challenges associated with the technology, and the development strategy for the next decade is still under debate.⁴⁹ However, with the recent and first demonstration of quantum generation of an entangled THz photon,²⁶ this latest assertion of the limited capability of photonics-based THz solutions for communication purposes may change dramatically in the coming years. That said, having an emitter capable of modulating and generating packets of parallel-encoded THz pulses without the need for an ultrafast electronic modulator will also be extremely useful in accelerating the development of new synchronous photonic solutions for sub-picosecond information detection without the need for fast electronic tools.

SUPPLEMENTARY MATERIAL

In the [supplementary material](#), details are provided on the pump beam image after the echelon mirror and DMD device. The pump intensity profile is compared to the generated THz pulse train. A simulation of the pump reflection after the echelon mirror is also used to illustrate the formation of the optical pulse train passing through the focal point of a lens.

ACKNOWLEDGMENTS

F.B. gratefully acknowledges financial support from the NSERC (Grant No. 2016-05020) and the Canada Research Chair (Grant No. CRC-2019-127). This research was also supported by FRQNT, which funds the activities of the COPL (Center d'Optique, Photonique et Laser) and RQMP (Regroupement Québécois sur les Matériaux

de Pointe) strategic clusters with which some of the authors are associated.

AUTHOR DECLARATIONS

Conflict of Interest

The authors have no conflicts to disclose.

Author Contributions

Joel Edouard Nkeck: Conceptualization (equal); Investigation (lead); Methodology (lead); Software (equal); Validation (lead). **Louis-Philip Béliveau:** Investigation (supporting); Software (lead). **Xavier Ropagnol:** Data curation (supporting); Methodology (supporting); Supervision (supporting); Validation (supporting); Writing – review & editing (supporting). **Dominic Deslandes:** Conceptualization (supporting); Methodology (supporting); Validation (equal); Writing – review & editing (supporting). **Denis Morris:** Formal analysis (equal); Resources (equal); Validation (equal); Writing – review & editing (supporting). **François Blanchard:** Conceptualization (equal); Data curation (equal); Funding acquisition (equal); Investigation (equal); Methodology (equal); Project administration (lead); Supervision (lead); Validation (lead); Writing – original draft (lead); Writing – review & editing (lead).

DATA AVAILABILITY

Data underlying the results presented in this paper are not publicly available at this time, but may be obtained from the authors upon reasonable request.

REFERENCES

- 1T. S. Rappaport, Y. Xing, O. Kanhere, S. Ju, A. Madanayake, S. Mandal, A. Alkhateeb, and G. C. Trichopoulos, "Wireless communications and applications above 100 GHz: Opportunities and challenges for 6G and beyond," *IEEE Access* **7**, 78729–78757 (2019).
- 2M. Tonouchi, "Cutting-edge terahertz technology," *Nat. Photonics* **1**, 97–105 (2007).
- 3S. S. Dhillon, M. S. Vitiello, E. H. Linfield, A. G. Davies, M. C. Hoffmann, J. Booske, C. Paoloni, M. Gensch, P. Weightman, G. P. Williams *et al.*, "The 2017 terahertz science and technology roadmap," *J. Phys. D Appl. Phys.* **50**, 043001 (2017).
- 4R. A. Lewis, "A review of terahertz sources," *J. Phys. D: Appl. Phys.* **47**, 374001 (2014).
- 5H. A. Hafez, X. Chai, A. Ibrahim, S. Mondal, D. Férachou, X. Ropagnol, and T. Ozaki, "Intense terahertz radiation and their applications," *J. Opt.* **18**, 093004 (2016).
- 6Y. Zhang, K. Li, and H. Zhao, "Intense terahertz radiation: Generation and application," *Front. Optoelectron.* **14**, 4–36 (2021).
- 7L. Guiramand, J. E. Nkeck, X. Ropagnol, T. Ozaki, and F. Blanchard, "Near-optimal intense and powerful terahertz source by optical rectification in lithium niobate crystal," *Photonics Res.* **10**, 340–346 (2022).
- 8R. A. Lewis, "A review of terahertz detectors," *J. Phys. D: Appl. Phys.* **52**, 433001 (2019).
- 9J. E. Nkeck, X. Ropagnol, R. Nechache, and F. Blanchard, "Electro-optical detection of terahertz radiation in a zinc sulphide crystal at a wavelength of 512 nm," *Appl. Phys. Express* **13**, 112007 (2020).
- 10H. Sakai, K. Kawase, and K. Murate, "Highly sensitive multi-stage terahertz parametric detector," *Opt. Lett.* **45**, 3905–3908 (2020).

- ¹¹J. Ajayan, D. Nirmal, R. Mathew, D. Kurian, P. Mohankumar, L. Arivazhagan, and D. Ajitha, "A critical review of design and fabrication challenges in InP HEMTs for future terahertz frequency applications," *Mater. Sci. Semicond. Process.* **128**, 105753 (2021).
- ¹²J. B. Baxter and G. W. Guglietta, "Terahertz spectroscopy," *Anal. Chem.* **83**, 4342–4368 (2011).
- ¹³M. G. Burdanova, A. P. Tsapenko, M. V. Kharlamova, E. I. Kauppinen, B. P. Gorshunov, J. Kono, and J. Lloyd-Hughes, "A review of the terahertz conductivity and photoconductivity of carbon nanotubes and heteronanotubes," *Adv. Opt. Mater.*, **9** 2101042 (2021).
- ¹⁴Y. Peng, C. Shi, Y. Zhu, M. Gu, and S. Zhuang, "Terahertz spectroscopy in biomedical field: A review on signal-to-noise ratio improvement," *Photonix* **1**, 12 (2020).
- ¹⁵M. Wan, J. J. Healy, and J. T. Sheridan, "Terahertz phase imaging and biomedical applications," *Opt. Laser Technol.* **122**, 105859–105871 (2020).
- ¹⁶B. Cheng, Z. Cui, B. Lu, Y. Qin, Q. Liu, P. Chen, Y. He, J. Jiang, X. He, X. Deng, J. Zhang, and L. Zhu, "340-GHz 3-D imaging radar with 4Tx-16Rx MIMO array," *IEEE Trans. THz Sci. Technol.* **8**(5), 509–519 (2018).
- ¹⁷C. Ottaviani, M. J. Woolley, M. Erementchouk, J. F. Federici, P. Mazumder, S. Pirandola, and C. Weedbrook, "Terahertz quantum cryptography," *IEEE J. Sel. Areas Commun.* **38**, 483–495 (2020).
- ¹⁸T. Nagatsuma, G. Ducournau, and C. C. Renaud, "Advances in terahertz communications accelerated by photonics," *Nat. Photonics* **10**, 371–379 (2016).
- ¹⁹R. Xu, S. Gao, B. S. Izquierdo, C. Gu, P. Reynaert, A. Standaert, G. J. Gibbons, W. Bosch, M. E. Gadringer, and D. Li, "A review of broadband low-cost and high-gain low-terahertz antennas for wireless communications applications," *IEEE Access* **8**, 57615–57629 (2020).
- ²⁰B. Ji, Y. Han, S. Liu, F. Tao, G. Zhang, Z. Fu, and C. Li, "Several key technologies for 6G: Challenges and opportunities," *IEEE Commun. Stand. Mag.* **5**, 44–51 (2021).
- ²¹S. Preu, G. H. Döhler, S. Malzer, L. J. Wang, and A. C. Gossard, "Tunable, continuous-wave terahertz photomixer sources and applications," *J. Appl. Phys.* **109**, 061301 (2011).
- ²²K. Nallappan, H. Guerboukha, C. Nerguizian, and M. Skorobogatiy, "Live streaming of uncompressed HD and 4K videos using terahertz wireless links," *IEEE Access* **6**, 58030–58042 (2018).
- ²³Y. Liu, S.-G. Park, and A. M. Weiner, "Terahertz waveform synthesis via optical pulse shaping," *IEEE J. Sel. Top. Quantum Electron.* **2**, 709–719 (1996).
- ²⁴A. M. Weiner, "Ultrafast optical pulse shaping: A tutorial review," *Opt. Commun.* **284**, 3669–3692 (2011).
- ²⁵See <https://cordis.europa.eu/project/id/965124> for information on a fully integrated chip-scale laser project with applications in engineering technologies.
- ²⁶M. Kutas, B. Haase, P. Bickert, F. Riexinger, D. Molter, and G. von Freymann, "Terahertz quantum sensing," *Sci. Adv.* **6**, eaz8065 (2020).
- ²⁷L. Liu, X. Zhang, M. Kenney, X. Su, N. Xu, C. Ouyang, Y. Shi, J. Han, W. Zhang, and S. Zhang, "Broadband metasurfaces with simultaneous control of phase and amplitude," *Adv. Mater.* **26**(29), 5031–5036 (2014).
- ²⁸G. R. Keiser, N. Karl, P. Q. Liu, C. Tulloss, H.-T. Chen, A. J. Taylor, I. Brener, J. L. Reno, and D. M. Mittleman, "Nonlinear terahertz metamaterials with active electrical control," *Appl. Phys. Lett.* **111**(12), 121101 (2017).
- ²⁹M. R. Hashemi, S. Cakmakyapan, and M. Jarrahi, "Reconfigurable metamaterials for terahertz wave manipulation," *Rep. Prog. Phys.* **80**, 094501 (2017).
- ³⁰S. Keren-Zur and T. Ellenbogen, "Direct space to time terahertz pulse shaping with nonlinear metasurfaces," *Opt. Express* **27**, 20837–20847 (2019).
- ³¹X. Ropagnol, E. Isgandarov, X. Chai, S. M. Raeis-Zadeh, S. Safavi-Naeini, M. Reid, F. Blanchard, and T. Ozaki, "Generation of intense sub-cycle terahertz pulses with variable elliptical polarization," *Appl. Phys. Lett.* **120**, 171106 (2022).
- ³²J. Ahn, A. Efimov, R. Averitt, and A. Taylor, "Terahertz waveform synthesis via optical rectification of shaped ultrafast laser pulses," *Opt. Express* **11**, 2486 (2003).
- ³³M. Sato, T. Higuchi, N. Kanda, K. Konishi, K. Yoshioka, T. Suzuki, K. Misawa, and M. Kuwata-Gonokami, "Terahertz polarization pulse shaping with arbitrary field control," *Nat. Photonics* **7**, 724–731 (2013).
- ³⁴Q. Tian, H. Xu, Y. Wang, Y. Liang, Y. Tan, X. Ning, L. Yan, Y. Du, R. Li, J. Hua, W. Huang, and C. Tang, "Efficient generation of a high-field terahertz pulse train in bulk lithium niobate crystals by optical rectification," *Opt. Express* **29**, 9624–9634 (2021).
- ³⁵S. Vidal, J. Degert, J. Oberlé, and E. Freysz, "Femtosecond optical pulse shaping for tunable terahertz pulse generation," *JOSA B* **27**, 1044–1050 (2010).
- ³⁶L. Gingras and D. G. Cooke, "Direct temporal shaping of terahertz light pulses," *Optica* **4**, 1416–1420 (2017).
- ³⁷V. Stummer, T. Flöry, G. Krizsán, G. Polónyi, E. Kaksis, A. Pugžlys, J. Hebling, J. A. Fülöp, and A. Baltuška, "Programmable generation of terahertz bursts in chirped-pulse laser amplification," *Optica* **7**, 1758–1763 (2020).
- ³⁸V. Muhammed, D. Mengu, N. T. Yardimci, Y. Luo, J. Li, Y. Rivenson, M. Jarrahi, and A. Ozcan, "Terahertz pulse shaping using diffractive surfaces," *Nat. Commun.* **12**, 1–13 (2021).
- ³⁹T. Seifert, S. Jaiswal, U. Martens, J. Hannegan, L. Braun, P. Maldonado, F. Freimuth, A. Kronenberg, J. Henrizi, I. Radu, E. Beaufort, Y. Mokrousov, P. M. Oppeneer, M. Jourdan, G. Jakob, D. Turchinovich, L. M. Hayden, M. Wolf, M. Münzenberg, M. Kläui, and T. Kampfrath, "Efficient metallic spintronic emitters of ultrabroadband terahertz radiation," *Nat. Photonics* **10**, 483–488 (2016).
- ⁴⁰Y. Minami, Y. Hayashi, J. Takeda, and I. Katayama, "Single-shot measurement of a terahertz electric-field waveform using a reflective echelon mirror," *Appl. Phys. Lett.* **103**(5), 051103 (2013).
- ⁴¹T. Makihara, K. Hayashida, G. T. No II, X. Li, N. Marquez Peraca, X. Ma, Z. Jin, W. Ren, G. Ma, I. Katayama, J. Takeda, H. Nojiri, D. Turchinovich, S. Cao, M. Bamba, and J. Kono, "Ultrastrong magnon-magnon coupling dominated by antiresonant interactions," *Nat. Commun.* **12**, 3115 (2021).
- ⁴²B. K. Ofori-Okai, P. Sivarajah, W. Ronny Huang, and K. A. Nelson, "THz generation using a reflective stair-step echelon," *Opt. Express* **24**, 5057–5068 (2016).
- ⁴³J. Zhao, J. Dai, B. Braverman, X.-C. Zhang, and R. W. Boyd, "Compressive ultrafast pulse measurement via time-domain single-pixel imaging," *Optica* **8**, 1176–1185 (2021).
- ⁴⁴K. Murate, M. J. Roshtkhari, X. Ropagnol, and F. Blanchard, "Adaptive spatiotemporal optical pulse front tilt using a digital micromirror device and its terahertz application," *Opt. Lett.* **43**, 2090–2093 (2018).
- ⁴⁵G. Torosyan, S. Keller, L. Scheuer, R. Beigang, and E. T. Papaioannou, "Optimized spintronic terahertz emitters based on epitaxial grown Fe/Pt layer structures," *Sci. Rep.* **8**(1), 1311 (2018).
- ⁴⁶A. Möhl and U. Fuchs, "Exploring the unlimited possibilities of modular aspheric Gauss to top-hat beam shaping," *Adv. Opt. Technol.* **5**, 201–210 (2016).
- ⁴⁷M. He, M. Xu, Y. Ren, J. Jian, Z. Ruan, Y. Xu, S. Gao, S. Sun, X. Wen, L. Zhou, L. Liu, C. Guo, H. Chen, S. Yu, L. Liu, and X. Cai, "High-performance hybrid silicon and lithium niobate Mach-Zehnder modulators for 100 Gbit s⁻¹ and beyond," *Nat. Photonics* **13**, 359–364 (2019).
- ⁴⁸T. Nagatsuma, A. Hirata, Y. Royter, M. Shinagawa, T. Furuta, T. Ishibashi, and H. Ito, *A 120-GHz Integrated Photonic Transmitter* (IEEE, 2000).
- ⁴⁹I. F. Akyildiz, C. Han, Z. Hu, S. Nie, and J. M. Jornet, "Terahertz band communication: An old problem revisited and research directions for the next decade," *IEEE Trans. Commun.* **70**(6), 4250–4285 (2022).
- ⁵⁰E. T. Papaioannou and R. Beigang, "THz spintronic emitters: A review on achievements and future challenges," *Nanophotonics* **10**, 1243–1257 (2021).